INFORMATION THEORY OF RADAR AND SONAR WAVEFORMS

Radar and active sonar systems extract information about an environment by illuminating it with electromagnetic or acoustic radiation. The illuminating field is scattered by objects in the environment, and the scattered field is collected by a receiver, which processes it to determine the presence, positions, velocities, and scattering characteristics of these objects. These active pulse-echo systems provide us with tools for observing environments not easily perceived using our senses alone. The key idea in any pulse-echo measurement system is to transmit a pulse or waveform and listen for the echo. Information about the scattering objects is extracted by comparing the transmitted pulse or waveform with the received waveform scattered by the object. Many characteristics, including the delay between transmission and reception, the amplitude of the echo, and changes in the shape of the transmitted waveform, are useful in providing information about the scattering objects.

Two primary attributes characterizing the echo return in a pulse-echo system are the round-trip propagation delay and the change in the received waveform resulting from the Doppler effect. The Doppler effect induces a compression or dilation in time for the scattered signal as a result of radial target motion toward or away from the pulse-echo sensor. For narrowband signals normally encountered in radar and narrowband active sonar systems, this is well approximated by a shift in the scattered waveform's center or carrier frequency proportional to the carrier frequency and the closing radial velocity between the target and scatterer (1). For wideband signals encountered in impulse radar and wideband sonar systems, this approximation is not accurate, and the Doppler effect must be modeled explicitly as a contraction or dilation of the time axis of the received signal.

One of the chief functions of a radar or sonar system is to distinguish, resolve, or separate the scattered returns from targets in the illuminated environment. This can be done by resolving the scatterers in delay, Doppler, or both delay and Doppler. In many problems of practical importance, resolution in delay or Doppler alone is not sufficient to achieve the desired resolution requirements for the pulse-echo measurement system. In these cases, joint delay-Doppler resolution is essential. The resolution capabilities of any pulse-echo system are a strong function of the shape of the transmitted waveforms employed by the system.

In the course of early radar development, radar systems were designed to measure the delay—and hence range—to the target, or they were designed to measure the Doppler frequency shift—and hence radial velocity—of the target with respect to the radar. The waveforms used for range measurement systems consisted of very narrow pulses for which the time delay between transmission and reception could easily be measured; these systems are referred to as *pulsed radar systems*. The waveforms used in the pulsed delay measurement radars were narrow pulses, with the ability to resolve closely spaced targets determined by the narrowness of the the pulses. If the returns from two pulses overlapped because two targets were too close to each other in range, the targets could not be resolved. So from a range resolution point of view, narrow pulses were considered very desirable. However, because the ability to detect small targets at a distance depends on the total energy in a pulse, it is not generally possible to make the pulses arbitrarily narrow and still achieve the necessary pulse energy without requiring unrealistic instantaneous power from the transmitter.

As radar systems theory and development progressed, it became clear that it was not pulse width per se that determined the delay resolution characteristics of a radar waveform, but rather the bandwidth of the transmitted radar signal. As a result, waveforms of longer duration—but appropriately modulated to achieve the necessary bandwidth to meet the desired delay resolution requirements—could be employed, which would allow for both sufficient energy to meet detection requirements and sufficient bandwidth to meet delay resolution requirements. The first detailed studies of waveforms with these properties were conducted by Woodward and Davies (2).

MATCHED FILTER PROCESSING

Radar systems typically process scattered target returns for detection by filtering of the received signal with a bank of matched filters matched to various time delayed and Doppler shifted versions of the transmitted signal. It is well known that a matched filter—or the corresponding correlation receiver—provides the maximum signal-to-noise ratio of all linear time-invariant receiver filters when the signal is being detected in additive white noise. Of course, if the filter is mismatched in delay or Doppler, the response, and hence signal-to-noise ratio, of the output will no longer be maximum. While this suboptimality of mismatched filters can in some cases be detrimental (e.g., where processing constraints only allow for a small number of Doppler filters), it provides the basis for target resolution in matched filter radar. We will now see how this gives rise to the notion of the ambiguity function—a key tool in radar resolution and accuracy assessment.

Let $s(t)$ be the baseband analytic signal transmitted by the radar system. After being demodulated down to baseband, the received signal due to a scatterer with round-trip delay τ_0 and Doppler frequency shift ν_0 is

$$r(t) = s(t-\tau_0)e^{j2\pi\nu_0 t}\, e^{j\phi}$$

where $e^{j\phi}$ is the phase shift in the received carrier due to the propagation delay τ_0; hence, $\phi = 2\pi f_0 \tau_0$. If we process this signal with a matched filter

$$h_{\tau,\nu}(t) = s^*(T-t+\tau)e^{-j2\pi\nu(T-t)}$$

matched to the signal

$$q(t) = s(t-\tau)e^{j2\pi\nu t}$$

and designed to maximize the signal output at time T, the matched filter output at time T is given by

$$\begin{aligned}
\mathcal{O}_T(\tau,\nu) &= \int_{-\infty}^{\infty} r(t)h_{\tau,\nu}(T-t)\,dt \\
&= \int_{-\infty}^{\infty} s(t-\tau_0)e^{j2\pi\nu_0 t}\, e^{j\phi} s^*(t-\tau)e^{-j2\pi\nu t}\,dt \\
&= e^{j\phi}\int_{-\infty}^{\infty} s(u)e^{j2\pi\nu_0(u+\tau_0)}s^*(u-(\tau-\tau_0))e^{-j2\pi\nu(u+\tau_0)}\,du \\
&= e^{j\phi}e^{-j2\pi(\nu-\nu_0)\tau_0}\int_{-\infty}^{\infty} s(u)s^*(u-(\tau-\tau_0))e^{-j2\pi(\nu-\nu_0)u}\,du \\
&= e^{j\phi}e^{-j2\pi(\nu-\nu_0)\tau_0}\chi_s(\tau-\tau_0,\ \nu-\nu_0)
\end{aligned}$$

where $\chi_s(\tau, \nu)$ is the *ambiguity function* of $s(t)$, defined as

$$\chi_s(\tau,\nu) = \int_{-\infty}^{\infty} s(t)s^*(t-\tau)e^{j2\pi\nu t}\,dt$$

For narrowband signals, $\nu\tau_0 \ll 1$ and $\nu_0\tau_0 \ll 1$ for all ν, ν_0, and τ_0 of interest, however, $f_0\tau_0 \gg 1$. Hence, we can write

$$\mathcal{O}_T(\tau,\nu) = e^{-j\phi}\chi_s(\tau-\tau_0,\ \nu-\nu_0) \tag{1}$$

Because $h_{\tau,\nu}(t)$ is a linear time-invariant filter, if we have N scatterers with scattering strengths $\mu_1, \ldots, \mu_N$, delays $\tau_1, \ldots, \tau_N$, and Doppler shifts $\nu_1, \ldots, \nu_N$, the response of $h_{\tau,\nu}(t)$ to the collection of scatterers is

$$\mathcal{O}_T(\tau,\nu) = \sum_{i=1}^{N}\mu_i e^{-j\phi_i}\chi_s(\tau-\tau_i,\ \nu-\nu_i)$$

where ϕ_i is the carrier phase shift in the return from the ith scatterer resulting from the propagation delay τ_i. Furthermore, if $\mu(\tau, \nu)$ describes a continuous scattering density, the response of the matched filter $h_{\tau,\nu}(t)$ to this scattering density is

$$\mathcal{O}_T(\tau,\nu) = \int_{-\infty}^{\infty}\int_{-\infty}^{\infty}\mu(t,v)e^{-j\phi(t)}\chi_s(\tau-t,\ \nu-v)\,dt\,dv$$

Here, $\phi(\tau) = e^{j2\pi f_0\tau}$ is the carrier phase shift caused by the propagation delay τ. If we define $\gamma(\tau, \nu) = \mu(\tau, \nu)e^{-j2\pi f_0\tau}$, this becomes

$$\mathcal{O}_T(\tau,\phi) = \int_{-\infty}^{\infty}\int_{-\infty}^{\infty}\gamma(t,v)\chi_s(\tau-t,\ \nu-v)\,dt\,dv$$

which is the two-dimensional convolution of $\gamma(\tau, \nu)$ with $\chi_s(\tau, \nu)$, and can be thought of as the image of $\gamma(\tau, \nu)$ obtained using an imaging aperture with point-spread function $\chi(\tau, \nu)$ (3, Chap. 4), as shown in Fig 1.

THE AMBIGUITY FUNCTION

As we have seen, the ambiguity function plays a significant role in determining the delay-Doppler resolution of a radar system. The ambiguity function was originally introduced by Woodward (2), and several related but functionally equivalent forms have been used since that time. Two common forms currently used are the *asymmetric ambiguity function* and the *symmetric ambiguity function,* and they are defined as follows. The *asymmetric ambiguity function* of a signal $s(t)$ is defined as

$$\chi_s(\tau,\nu) = \int_{-\infty}^{\infty} s(t)s^*(t-\tau)e^{j2\pi\nu t}\,dt \tag{2}$$

and the *symmetric ambiguity function* of $s(t)$ is defined as

$$\Gamma_s(\tau,\nu) = \int_{-\infty}^{\infty} s(t+\tau/2)s^*(t-\tau/2)e^{-j2\pi\nu t}\,dt \tag{3}$$

The notation "*" denotes complex conjugation. The asymmetric ambiguity function is the form typically used by radar engineers and most closely related to the form introduced by Woodward (2). The symmetric ambiguity function is more widely used in signal theory because its symmetry is mathematically convenient and it is consistent with the general theory of time–frequency distributions (4).

The asymmetric ambiguity function $\chi_s(\tau, \nu)$ and the symmetric ambiguity function $\Gamma_s(\tau, \nu)$ are related by

$$\Gamma_s(\tau,\nu) = e^{j\pi\nu t}\chi_s(\tau,\ -\nu)$$

and

$$\chi_s(\tau,\nu) = e^{j\pi\nu t}\Gamma_s(\tau,\ -\nu)$$

so knowledge of one form implies knowledge of the other. In practice, the *ambiguity surface* $A_s(\tau, \nu)$, given by the modulus of the symmetric ambiguity function,

$$A_s(\tau,\nu) = |\Gamma_s(\tau,\nu)| = |\chi_s(\tau,\ -\nu)|$$

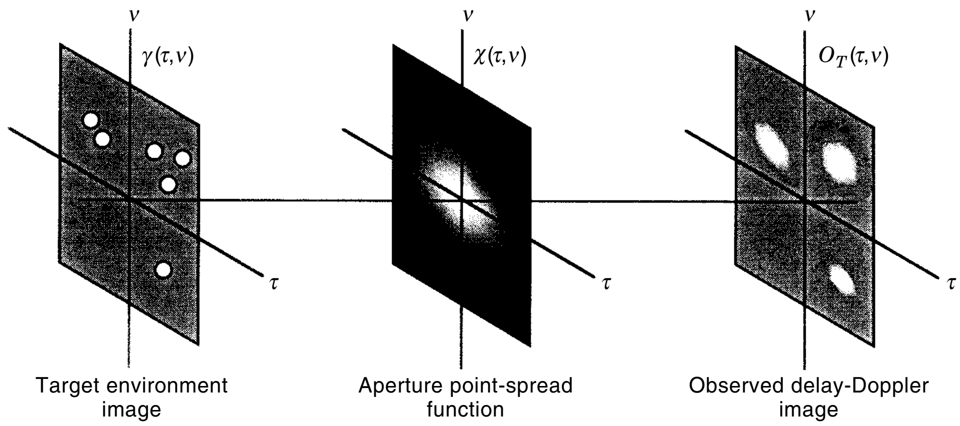

Figure 1. Imaging interpretation of a delay-Doppler pulse-echo system. A waveform $s(t)$ with ambiguity function $\chi(\tau, \nu)$ gives rise to a delay-Doppler image $\mathcal{O}_T(\tau, \nu)$ that is the convolution of the ideal image $\gamma(\tau, \nu)$ with the point-spread function $\chi(\tau, \nu)$.

is usually sufficient to characterize a waveform's delay-Doppler resolution characteristics, as it gives the magnitude of the matched filter response for a delay-Doppler mismatch of (τ, ν).

Figures 2 and 3 show ambiguity surfaces of a simple pulse

$$s_1(t) = \begin{cases} 1, & \text{for } |t| < 1/2 \\ 0, & \text{elsewhere} \end{cases}$$

and a linear FM "chirp"

$$s_2(t) = \begin{cases} e^{j\pi\alpha t^2}, & \text{for } |t| < 1/2 \\ 0, & \text{elsewhere} \end{cases}$$

(with $\alpha = 8$), respectively. The ambiguity function of $s_1(t)$ is

$$\Gamma_{s_1}(\tau,\ \nu) = \begin{cases} (1-|\tau|)\mathrm{sinc}[\nu(1-|\tau|)], & \text{for } |\tau| \le 1 \\ 0, & \text{elsewhere} \end{cases}$$

The ambiguity function of $s_2(t)$ is

$$\Gamma_{s_2}(\tau,\ \nu) = \begin{cases} (1-|\tau|)\mathrm{sinc}[(\nu-\alpha\tau)(1-|\tau|)], & \text{for } |\tau| \le 1 \\ 0, & \text{elsewhere} \end{cases}$$

These figures illustrate the very different delay-Doppler resolution characteristics provided by these signals when they are processed using a matched filter.

The shape or properties of the main lobe of the ambiguity surface $|\Gamma_s(\tau,\ \nu)|$ centered about the origin determine the ability of the corresponding waveform to resolve two scatterers close together in both delay and Doppler. The ambiguity surface squared $|\Gamma_s(\tau,\ \nu)|^2$ close to the origin can be expanded as a two-dimensional Taylor series about $(\tau,\ \nu) = (0,\ 0)$. From this it follows that the ambiguity surface itself may be approximated by (8, pp. 21–22)

$$|\Gamma_s(\tau,\ \nu)| \approx \Gamma(0,\ 0)[1 - 2\pi^2 T_{\mathrm{G}}^2 \nu^2 - 4\pi\rho T_{\mathrm{G}} B_{\mathrm{G}} \tau\nu - -2\pi^2 B_{\mathrm{G}}^2 \tau^2] \tag{4}$$

where

$$B_{\mathrm{G}} = \sqrt{\overline{f^2} - \overline{f}^2}$$

is the *Gabor bandwidth* of the signal,

$$T_{\mathrm{G}} = \sqrt{\overline{t^2} - \overline{t}^2}$$

is the *Gabor timewidth* of the signal, the frequency and time

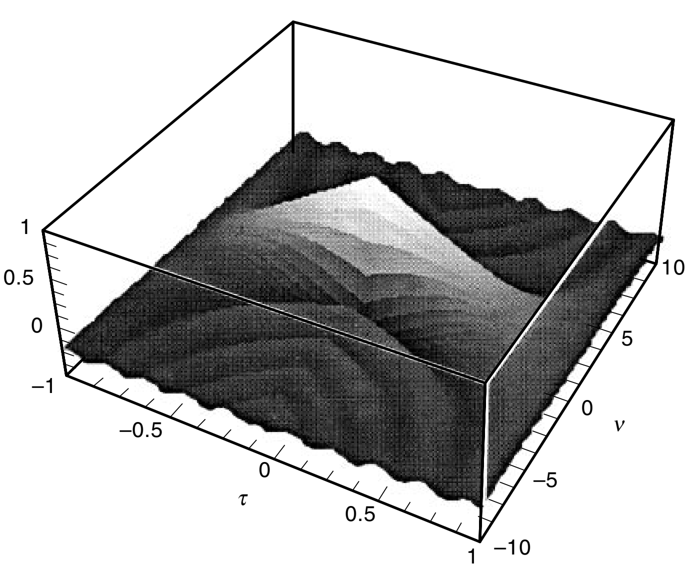

Figure 2. Symmetric ambiguity function $\Gamma_1(\tau,\ \nu)$ of a rectangular pulse of duration 1.

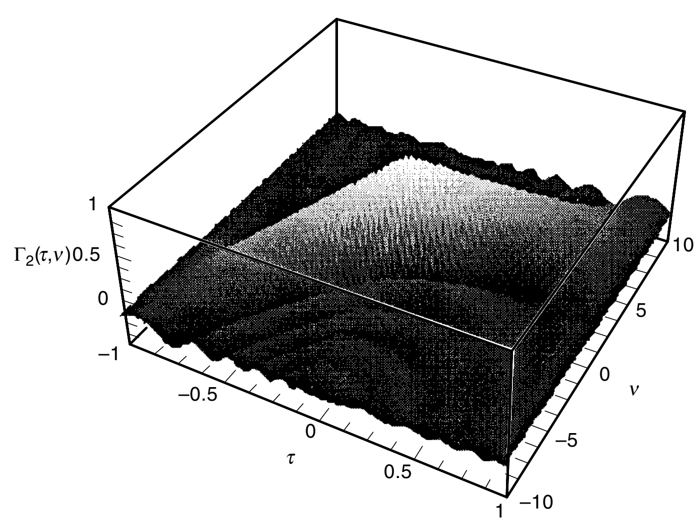

Figure 3. Symmetric ambiguity function $\Gamma_2(\tau,\ \nu)$ of a linear FM chirp of duration 1.

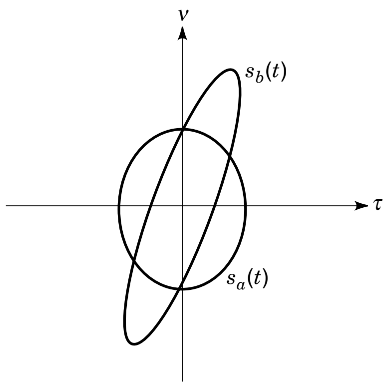

Figure 4. Uncertainty ellipses corresponding to $s_a(t) = e^{-\beta t^2}$ and $s_b(t) = e^{-\beta t^2} e^{j\pi\alpha t^2}$.

moments of the signal $s(t)$ are

$$\overline{f^n} = \frac{1}{E_s} \int_{-\infty}^{\infty} f^n |S(f)|^2 \, df$$

and

$$\overline{t^n} = \frac{1}{E_s} \int_{-\infty}^{\infty} t^n |s(t)|^2 \, dt$$

respectively, and the *skew parameter* ρ is

$$\rho = \frac{1}{TB} \operatorname{Re}\left\{ \frac{j}{2\pi E_s} \int_{-\infty}^{\infty} t\dot{s}(t) s^*(t) \, dt - \overline{t}\,\overline{f} \right\}$$

where $\dot{s}(t)$ is the derivative of $s(t)$.

The shape of the main lobe about the origin of the ambiguity function can be determined by intersecting a plane parallel to the (τ, ν) plane with the main lobe near the peak value. Using the approximation of Eq. (4) and setting it equal to the constant ambiguity surface height γ_0 specified by the intersecting plane, we have

$$\Gamma(0, 0)[1 - 2\pi^2 T_{\mathrm{G}}^2 \nu^2 - 4\pi\rho T_{\mathrm{G}} B_{\mathrm{G}} \tau\nu - 2\pi^2 B_{\mathrm{G}}^2 \tau^2] = \gamma_0$$

which we can rewrite as

$$B_{\mathrm{G}}^2 \tau^2 + 2\rho B_{\mathrm{G}} T_{\mathrm{G}} \tau\nu + T_{\mathrm{G}}^2 \nu^2 = C \tag{5}$$

where C is a positive constant. This is the equation of an ellipse in τ and ν, and this ellipse is known as the *uncertainty ellipse* of the waveform $s(t)$. The uncertainty ellipse describes the shape of the main lobe of $|\Gamma_s(\tau, \nu)|$ in the region around its peak and hence provides a concise description of the capability of $s(t)$ to resolve closely spaced targets concentrated in the main lobe region. The value of C itself is not critical, since the shape of the uncertainty ellipse is what is of primary interest. Figure 4 shows the uncertainty ellipses of a Gaussian pulse

$$s_a(t) = e^{-\beta t^2}$$

and a linear FM chirp modulated Gaussian pulse

$$s_b(t) = e^{-\beta t^2} e^{j\pi\alpha t^2}$$

While the uncertainty ellipse provides a rough means of determining the resolution performance of a waveform for resolving closely spaced targets in isolation from other interfering scatterers, it is not sufficient to completely characterize a waveform's measurement characteristics. Target returns with delay-Doppler coordinates falling in the sidelobes of the ambiguity function can have a significant effect on a radar's measurement and resolution capabilities. For this reason, in order to effectively design radar waveforms for specific measurement tasks, it is important to have a thorough understanding of the properties of ambiguity functions.

Properties of Ambiguity Functions

In order to gain a thorough understanding of the delay-Doppler resolution characteristics of various signals under matched filter processing, it is necessary to understand the general properties of ambiguity functions. With this in mind, we now consider the properties of ambiguity functions. Proofs of these properties may be found in Refs. 5 (Chap. 9), 6 (Chaps. 5–7), 7 (Chap. 4), 8, and 9 (Chap. 10).

Property 1. The energy in the signal $s(t)$ is given by

$$E_s = \Gamma_s(0, 0) = \int_{-\infty}^{\infty} |s(t)|^2 \, dt$$

Property 2 (Volume).

$$\int_{-\infty}^{\infty} \int_{-\infty}^{\infty} |\Gamma_s(\tau, \nu)|^2 \, d\tau \, d\nu = |\Gamma_s(0, 0)|^2 = E_s^2$$

Property 3. The *time autocorrelation function* $\phi_s(\tau)$ of the signal $s(t)$ is given by

$$\phi_s(\tau) = \Gamma_s(\tau, 0) = \int_{-\infty}^{\infty} s(t + \tau/2) s^*(t - \tau/2) \, dt$$

Property 4. The energy spectrum of the signal $s(t)$ is given by

$$\Gamma_s(0, \nu) = \int_{-\infty}^{\infty} |s(t)|^2 e^{-j2\pi\nu t} \, dt$$

Property 5. The symmetric ambiguity function of the signal $s(t)$ can be written as

$$\Gamma_s(\tau, \nu) = \int_{-\infty}^{\infty} S(f + \nu/2) S^*(f - \nu/2) e^{j2\pi f\tau} \, df$$

where

$$S(f) = \int_{-\infty}^{\infty} s(t) e^{-j2\pi ft} \, dt$$

is the Fourier transform of $s(t)$.

Property 6. If $s(0) \neq 0$, $s(t)$ can be recovered from $\Gamma_s(\tau, \nu)$ using the relationship

$$s(t) = \frac{1}{s^*(0)} \int_{-\infty}^{\infty} \Gamma_s(t, \nu) j\pi\nu t \, dt$$

where

$$|s(0)|^2 = \int_{-\infty}^{\infty} \Gamma_s(0,\ \nu)\, d\nu$$

Property 7 (Time Shift). Let $s'(t) = s(t - \Delta)$. Then

$$\Gamma_{s'}(\tau,\ \nu) = e^{-j2\pi\nu\Delta}\Gamma_s(\tau,\ \nu)$$

Property 8 (Frequency Shift). Let $s'(t) = s(t)e^{j2\pi ft}$. Then

$$\Gamma_{s'}(\tau,\ \nu) = e^{j2\pi f\tau}\Gamma_s(\tau,\ \nu)$$

Property 9 (Symmetry). $\Gamma_s(\tau, \nu) = \Gamma_s^*(-\tau, -\nu)$.

Property 10 (Maximum). The largest magnitude of the ambiguity function is always at the origin:

$$|\Gamma_s(\tau,\ \nu)| \le \Gamma_s(0,\ 0) = E_s$$

This follows directly from the Schwarz inequality.

Property 11 (Time Scaling). Let $s'(t) = s(at)$, where $a \neq 0$. Then

$$\Gamma_{s'}(\tau,\ \nu) = \frac{1}{|a|}\Gamma_s(a\tau,\ \nu/a)$$

Property 12 (Quadratic Phase Shift). Let $s'(t) = s(t)e^{j\pi\alpha t^2}$. Then

$$\Gamma_{s'}(\tau,\ \nu) = \Gamma_s(\tau,\ \nu - \alpha\tau)$$

Property 13 (Self-transform). $|\Gamma_s(\tau, \nu)|^2$ is its own Fourier transform in the sense that

$$\int_{-\infty}^{\infty}\int_{-\infty}^{\infty} |\Gamma_s(\tau,\ \nu)|^2 e^{-j2\pi f\tau}\, e^{j2\pi t\nu}\, d\tau\, d\nu = |\Gamma_s(t,\ f)|^2$$

Property 14 (Wigner Distribution). The two-dimensional inverse Fourier transform of the ambiguity function $\Gamma_s(\tau, \nu)$ of a signal $s(t)$ is its Wigner distribution $W_s(t, f)$:

$$\int_{-\infty}^{\infty}\int_{-\infty}^{\infty} \Gamma_s(\tau,\ \nu) e^{j2\pi f\tau}\, e^{j2\pi t\nu}\, d\tau\, d\nu = W_s(t,\ f)$$

where the Wigner distribution of $s(t)$ is defined as (4,8)

$$W_s(t,\ f) = \int_{-\infty}^{\infty} s(t + \tau/2)s^*(t - \tau/2)e^{j2pif\tau}\, d\tau$$

These properties of the ambiguity function have immediate implications for the design of radar waveforms. From the imaging analogy of delay-Doppler measurement, where the ambiguity function plays the role of the imaging aperture, it is clear that an ideal ambiguity function would behave much like a pinhole aperture—a two-dimensional Dirac delta function centered at the origin of the delay-Doppler plane. Such an ambiguity function would yield a radar system giving a response of unity if the return had the assumed delay and Doppler, but a response of zero if it did not. Such a system would in fact have perfect delay-Doppler resolution properties. Unfortunately, such an ambiguity function does not exist. This can be seen by considering Property 1 and Property 2 of the ambiguity function. Property 1 states that the height of $|\Gamma_s(\tau, \nu)|^2$ at the origin is $|\Gamma_s(0, 0)|^2 = E_s^2$. Property 2 states that the total volume under $|\Gamma_s(\tau, \nu)|^2$ is E_s^2. So if we try to construct a thumbtack-like $|\Gamma_s(\tau, \nu)|^2$ approximating an ideal delta function, we run into the problem that as the height $|\Gamma_s(0, 0)|$ increases, so does the volume under $|\Gamma_s(\tau, \nu)|^2$. This means that for a signal with a given energy, if we try to push the volume of the ambiguity function down in one region of the delay-Doppler plane, it must pop up somewhere else. So there are limitations on just how well any waveform can do in terms of overall delay-Doppler ambiguity performance. In fact, the radar waveform design problem corresponds to designing waveforms that distribute the ambiguity volume in the (τ, ν) plane in a way appropriate for the delay-Doppler measurement problem at hand. We now investigate some of these techniques.

The Wideband Ambiguity Function

In the situation that the waveforms being considered are not narrowband or the target velocity is not small compared with the velocity of wave propagation, the Doppler effect cannot be modeled accurately as a frequency shift. In this case, it must be modeled as a contraction or dilation of the time axis. When this is the case, the ambiguity functions $\chi_s(\tau, \nu)$ and $\Gamma_s(\tau, \nu)$ defined in Eqs. (2) and (3) can no longer be used to model the output response of the delay and Doppler (velocity) mismatched matched filter. In this case, the *wideband ambiguity function* must be used (10–13). Several slightly different but mathematically equivalent forms of the wideband ambiguity function have been introduced. One commonly used form (13) is

$$\Psi_s(\tau,\ \gamma) = \sqrt{|\gamma|}\int_{-\infty}^{\infty} s(t)s^*(\gamma(t - \tau))\, dt \tag{6}$$

where γ is the *scale factor* arising from the contraction or dilation of the time axis as a result of the Doppler effect. Specifically,

$$\gamma = \frac{1 - v/c}{1 + v/c}$$

where v is the radial velocity of the target with respect to the sensor (motion away from the sensor positive), and c is the velocity of wave propagation in the medium. While the theory of wideband ambiguity functions is not as well developed as for the case of narrowband ambiguity functions, a significant amount of work has been done in this area. See Ref. 13 for a readable survey of current results. We will focus primarily on the narrowband ambiguity function throughout the rest of this article.

RADAR WAVEFORM DESIGN

The problem of designing radar waveforms with good delay-Doppler resolution has received considerable attention (14–24). Waveforms developed for this purpose have generally fallen into three broad categories:

1. Phase and frequency modulation of individual radar pulses

2. Pulse train waveforms
3. Coded waveforms

We will now investigate these techniques and consider how each can be used to improve radar delay-Doppler resolution characteristics and shape the ambiguity functions of radar waveforms in desirable ways.

Phase and Frequency Modulation of Radar Pulses

The fundamental observation that led to the development of phase and frequency modulation of radar pulses was that it is not the duration of a pulse, but rather its bandwidth, that determines its range resolution characteristics. Early range measurement systems used short duration pulses to make range measurements, and narrow pulses were used to obtain good range resolution, but this put a severe limitation on the detection range of these systems, because detection performance is a function of the total energy in the transmitted pulse, and with the peak power limitations present in most real radar systems, the only way to increase total energy is to increase the pulse duration. However, if the pulse used is simply gating a constant frequency sinusoidal carrier, increasing the duration decreases the bandwidth of the transmitted signal. This observation led to the conjecture that perhaps it is large bandwidth instead of short pulse duration that leads to good range resolution. This conjecture was in fact shown to be true (14). We now investigate this using ambiguity functions.

The ambiguity function of the simple rectangular pulse

$$s_1(t) = \begin{cases} 1, & \text{for } |t| \le T \\ 0, & \text{elswhere} \end{cases}$$

of duration T is

$$\Gamma_1(\tau,\ \nu) = \begin{cases} (T - |\tau|)\text{sinc}[\nu(T - |\tau|)], & \text{for } |t| \le T \\ 0, & \text{elswhere} \end{cases}$$

and the ambiguity function of the linear FM "chirp" pulse

$$s_2(t) = \begin{cases} e^{j\pi\alpha t^2}, & \text{for } |t| \le T \\ 0, & \text{elswhere} \end{cases}$$

of the same duration is

$$\Gamma_2(\tau,\ \nu) = \begin{cases} (T - |\tau|)\text{sinc}[(\nu - \alpha\tau)(T - |\tau|)], & \text{for } |t| \le T \\ 0, & \text{elswhere} \end{cases}$$

[Note that $\Gamma_2(\tau,\ \nu)$ is easily obtained from $\Gamma_1(\tau,\ \nu)$ using Property 12 of the ambiguity function.] If we compare the time autocorrelation functions $\phi_1(\tau) = \Gamma_1(\tau,\ 0)$ and $\phi_2(\tau) = \Gamma_2(\tau,\ 0)$ for various values of the linear FM modulation index α as

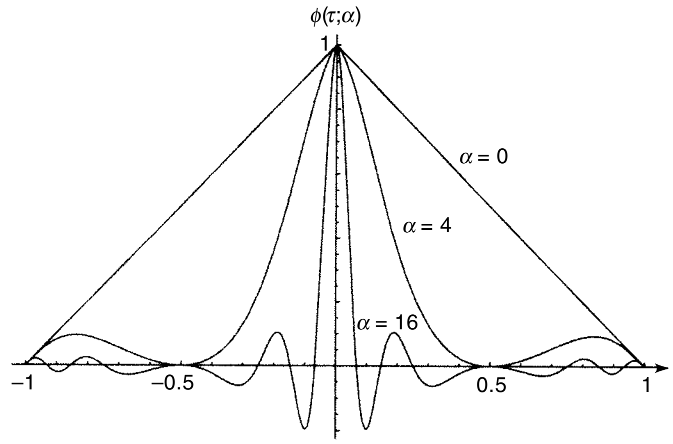

Figure 5. Time correlation $\phi(\tau,\ \alpha) = \Gamma_s(\tau,\ 0)$ for linear FM chirp pulses of duration 1 and modulation indices α of 0, 4, and 16.

shown in Fig. 5, we see that, although pulse durations are equivalent (in this case we take $T = 1$), there is a significant difference in range resolution. With increasing α, we also have increasing bandwidth. Looking at the ambiguity function of the linear FM chirp shown in Fig. 3, and comparing the ambiguity function of the simple rectangular pulse in Fig. 2, it is clear that the broadening of the pulse bandwidth has brought about increased delay resolution–however, not without cost.

From Property 12, the quadratic phase shift property, we see that the matched filter will not only have a large response to the signal with the desired delay τ and Doppler ν, but also to any signal with delay $\tau + \Delta\tau$ and Doppler $\nu + \Delta\nu$, where $\Delta\nu - \alpha\ \Delta\tau = 0$. This locus of peak response for the chirp is oriented along the line of slope α in the $(\tau,\ \nu)$ plane. So when matched filtering for a chirp with some desired delay and Doppler shift imposed on it, we are never certain if a large response is the result of a scatterer at the desired delay and Doppler, or a scatterer with a delay-Doppler offset lying near the locus of maximal delay-Doppler response. While for a single scatterer the actual delay and Doppler can be determined by processing with a sufficiently dense band of matched filters in delay and Doppler, scatterers lying along this maximal response locus are hard to resolve if they are too close in delay and Doppler. From the point of view of detection, however, there is a benefit to this "Doppler tolerance" of the chirp waveform. It is not necessary to have a bank of Doppler filters as densely located in Doppler frequency in order to detect the presence of targets (25, Chap. 9).

Coherent Pulse Train Waveforms

Another way to increase the delay-Doppler resolution and ambiguity characteristics of radar waveforms is through the use of pulse trains—waveforms synthesized by repeating a simple pulse shape over and over. An extension of this basic idea involves constructing the pulse train as a sequence of shorter waveforms—not all the same—from a prescribed set of waveforms (26). Most modern radar systems employ pulse trains instead of single pulses for a number of reasons. Regardless of whether the pulse train returns are processed coherently (keeping track of the phase reference from pulse-to-pulse and using it to construct a matched filter) or noncoherently (simply summing the pulse-to-pulse amplitude of the matched filter output without reference to phase), a pulse train increases receiver output signal-to-noise ratio, and hence increases detection range [e.g., see Ref. 25 (Chaps. 6 and 8)]. Furthermore, when processed coherently in a pulse-Doppler processor, flexible, high-resolution delay-Doppler processing is possible. In discussing pulse trains, we will focus on coherent pulse-Doppler waveforms, as pulse-Doppler radar systems have become the dominant form of radar for both surveillance and synthetic aperture radar (SAR) applications.

A pulse train is constructed by repeating a single pulse $p(t)$ regularly at uniform intervals T_r; T_r is called the *pulse repetition interval* (PRI). The frequency $f_r = 1/T_r$ is called the *pulse repetition frequency* (PRF) of the pulse train. Typically, the duration τ_p of the pulse $v(t)$ is much less than T_r. A uniform pulse train $s(t)$ made up of N repeated pulses and having PRI T_r can be written as

$$x(t) = \sum_{n=0}^{N-1} p(t - nT_r)$$

A typical example of such a pulse train in which the pulse $p(t)$ repeated is a simple rectangular pulse is shown in Fig. 6. Centering this pulse train about the origin of the time axis, we can write it as

$$s(t) = \sum_{n=0}^{N-1} p(t - nT_r + (N-1)T_r/2) \qquad (7)$$

The symmetric ambiguity function of this pulse train is (6,8)

$$\Gamma_s(\tau,\ \nu) = \sum_{n=-(N-1)}^{N-1} \left[\frac{\sin \pi \nu T_r (N - |n|)}{\sin \pi \nu T_r}\right] \cdot \Gamma_p(\tau - nT_r,\ \nu) \qquad (8)$$

where $\Gamma_p(\tau,\ \nu)$ is the ambiguity function of the elementary pulse $p(t)$ used to construct the pulse train.

In order to gain an understanding for the behavior of the ambiguity function of the pulse train, consider the special case of a uniform pulse train of $N = 5$ rectangular pulses, each of length $\tau_p = 1$ with a PRI of $T_r = 5$. The plot of this ambiguity function is shown in Fig. 7. A similar plot in which $p(t)$ is a linear FM chirp of the form

$$p(t) = \begin{cases} e^{j\pi\alpha t^2}, & \text{for } |t| \le 1 \\ 0, & \text{elsewhere} \end{cases}$$

and $\alpha = 8$ is shown in Fig. 8. From the form of Eq. (8), we see that the ambiguity function of the pulse train has "grating lobes" centered at $(\tau,\ \nu)$ pairs given by

$$(\tau,\ \nu) = (nT_r,\ k/T_r)$$

where n is any integer with $|n| \le N - 1$, and k is any integer. From the behavior of the Dirichlet function

$$\left[\frac{\sin \pi \nu T_r (N - |n|)}{\sin \pi \nu T_r}\right]$$

weighting the delayed copies of $\Gamma_p(\tau,\ \nu)$ in Eq. (8), it is clear that the peak amplitudes of these grating lobes fall off as we move farther away from the main lobe ($n = 0$ and $k = 0$).

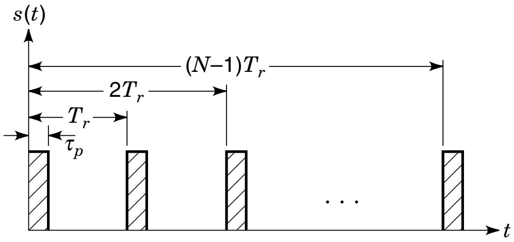

Figure 6. Uniform pulse train waveform $s(t)$ constructed by repeating a basic pulse shape $p(t)$ N times with a pulse repetition interval of T_r.

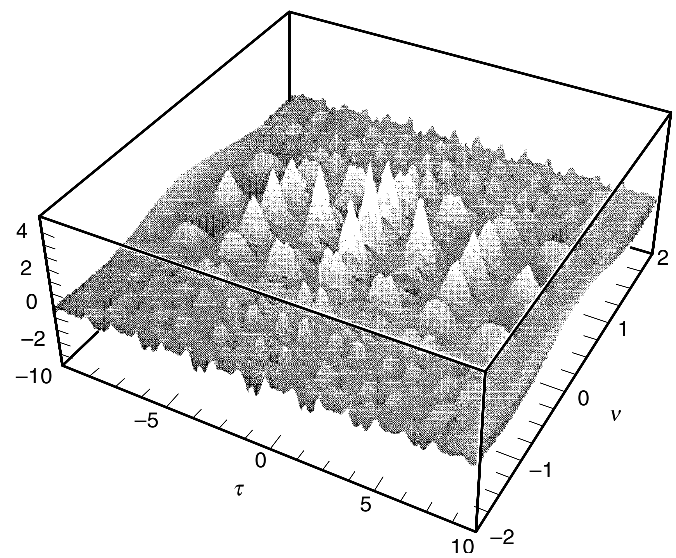

Figure 7. The ambiguity function for a uniform pulse train of rectangular pulses.

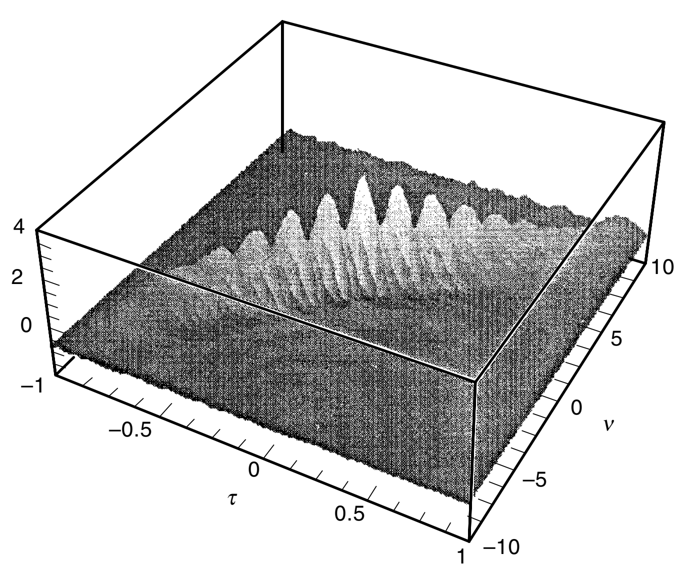

Figure 8. The ambiguity function for a uniform pulse train of linear FM chirp pulses.

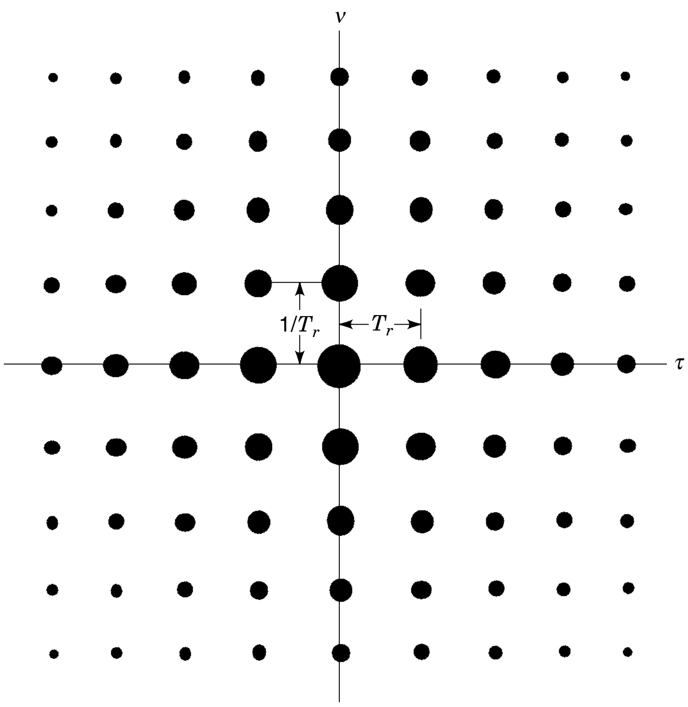

Figure 9. Locations of grating sidelobes in the ambiguity function of a uniform pulse train.

Figure 9 shows this grating lobe behavior for a uniform pulse train.

By observing the main lobe of the uniform pulse train, we see that its delay resolution is approximately τ_p—the range resolution of the elementary pulse $p(t)$—while the Doppler resolution is approximately $1/NT_r$, a value that can be made arbitrarily small by making N sufficiently large, limited only by practical considerations in coherently processing the received signal. However, the ambiguities introduced through the grating lobes at $(nT_r, k/T_r)$ can result in uncertainty in the actual delay and Doppler of the target. As a result, both the range and Doppler determined radial velocity of the target can be ambiguous. While in principle this ambiguity can be resolved in the case of a small number of targets using the fact that the sidelobes have successively smaller amplitude as we move away from the main lobe, this approach is not practical because of the way in which the bank of matched filters is actually implemented in a pulse-Doppler processor. Hence, another approach to resolving $(nT_r, k/T_r)$ ambiguity is needed. We will briefly discuss approaches that can be taken.

One way to reduce the effects of the range ambiguity is to make T_r large. This makes the delay ambiguity large, and often the delay ambiguity (and hence unambiguous measurement range) can be made sufficiently large so that range ambiguity is no longer a problem for ranges of interest. Of course, this complicates the Doppler ambiguity problem, because the pulse repetition frequency (PRF) $1/T_r$ is the effective sampling rate of the pulse-Doppler processor. A large value of T_p results in a low PRF and hence low sampling rate, and there is significant aliasing of the Doppler signal. Some systems do use this approach to deal with the ambiguity problem, using range differences (often called range rate measurements) from pulse to pulse to resolve the Doppler ambiguity; however, this approach is only successful in sparse target environments. When there are many targets in proximity in both delay and Doppler, sorting out the ambiguity becomes unwieldy. Another disadvantage of these *low PRF pulse trains* is that they have lower duty cycles for a given pulse width, resulting in a significant decrease in average transmitted power (and hence detection range) for a given elemental pulse width τ_p and peak power constraint.

At the other extreme, if one makes T_r very small, the effects of Doppler ambiguity can be minimized. In fact, if $1/T_r$ is greater than the maximum Doppler frequency shift we expect to encounter, there is no Doppler ambiguity. However, there will most likely be severe range ambiguities if such *high PRF pulse trains* are used.

For most radar surveillance problems involving the detection of aircraft and missiles, the size of the surveillance volume and the target velocities involved dictate that there will be ambiguities in both delay and Doppler, and most often a *medium PRF pulse train* is employed. In this case the PRF is usually selected to meet the energy efficiency (duty-cycle) constraints to ensure reliable detection and to make the nature of the delay-Doppler ambiguities such that they are not extreme in either the delay or Doppler dimension. In this case, delay-Doppler ambiguities can be resolved by changing the PRF from one coherent N-pulse train to the next by changing T_r from pulse train to pulse train. This technique is sometimes called *PRF staggering,* and is effective in sparse environments. As can be seen from Eq. (8), proper selection of the T_r from pulse train to pulse train makes this feasible, because in general, with proper selection of the PRIs T_r used, only the true delay-Doppler (τ, ν) will be a feasible solution for all T_r. An additional benefit of changing T_r from pulse train to pulse train is that it alleviates the "blind range" problem in monostatic radars. These radars cannot transmit and receive simultaneously. When they transmit a pulse train, the receiver is turned off during pulse transmission and is turned on to listen for target returns in the periods between pulses. Hence target returns having delays corresponding to the time intervals of successive pulse transmissions are not seen by the radar. Changing T_r from pulse train to pulse train moves the blind ranges around, ensuring nearly uniform surveillance coverage at all ranges.

Phase and Frequency Coded Waveforms

Another highly successful approach to designing waveforms with desirable ambiguity functions has been to use phase and/or frequency coding. The general form of a coded waveform (with coding in both phase and frequency) is

$$s(t) = \sum_{n=0}^{N-1} p_T(t - nT)\exp\{j2\pi d_n t/T\}\exp\{j\phi_n\} \tag{9}$$

The coded waveform $s(t)$ consists of a sequence of N identical baseband pulses $p_T(t)$ of length T; these pulses $p_T(t - nT)$ are usually referred to as the *chips* making up the waveform $s(t)$. Usually, the chip pulse $p_T(t)$ has the form

$$p_T(t) = \begin{cases} 1, & \text{for } 0 \le t < T \\ 0, & \text{elsewhere} \end{cases}$$

Note that each chip pulse $p_T(t - nT)$ is of duration T and each successive pulse is delayed by T, so there are no empty spaces in the resulting coded waveform $s(t)$ of duration NT. In fact, for the rectangular $p_T(t)$ specified above, $|s(t)| = 1$ for all $t \in [0, NT)$. However, each pulse in the sequence is modulated by an integral frequency modulating index d_n and a phase ϕ_n that can take on any real number value. To specify the modulating frequency and phase patterns of a coded waveform, we must specify a length N sequence of frequency indices $\{d_0, \ldots, d_{N-1}\}$ and a length N sequence of phases $\{\phi_0, \ldots, \phi_{N-1}\}$. If $d_n = 0$ for $n = 0, \ldots, N - 1$, then the coded waveform is strictly phase modulated. If $\phi_n = 0$ for $n = 0, \ldots, N - 1$, then the coded waveform is strictly frequency modulated. The asymmetric ambiguity function of $s(t)$ as given in Eq. (9) is given by (26)

$$\chi_s(\tau, \nu) = \sum_{n=0}^{N-1} \sum_{m=0}^{N-1} e^{j(\phi_n - \phi_m)} e^{j2\pi(d_m/T)\tau} e^{-j2\pi\nu nT} \chi_{p_T} \left(\tau - (n-m)T, \nu - \frac{(d_n - d_m)}{T}\right) \quad (10)$$

There are many families of coded phase and frequency modulated waveforms. We will consider a few of the most interesting of these. For a more thorough treatment of coded waveforms, see Refs. 5 (Chap. 6), 6 (Chap. 8), and 7 (Chap. 8).

Frequency Coded Waveforms. Consider an N-chip frequency coded waveform with the rectangular $p_T(t)$ defined above (here we assume $\phi_0 = \cdots = \phi_{N-1} = 0$):

$$s(t) = \sum_{n=0}^{N-1} p_T(t - nT) \exp\{j2\pi d_n t/T\} \quad (11)$$

Waveforms of this kind are sometimes referred to as *frequency hopping waveforms,* because the frequency of the waveform "hops" to a new frequency when transitioning from chip to chip. Now suppose we take the sequence of frequency modulation indices to be

$$\phi_n = n, \quad n = 0, \ldots, N - 1$$

Then the resulting $s(t)$ is a stepped frequency approximation to a linear FM chirp. Here we have used each of the frequency modulation indices in the set $\{0, \ldots, N - 1\}$ once and only once. In general, we can describe the order in which the indices are used to construct the waveform using a *frequency index sequence* of the form $(d_0, \ldots, d_{N-1})$. So, for example, the stepped linear FM sequence has frequency index sequence $(0, 1, 2, \ldots, N - 1)$. There are of course $N!$ possible frequency coded waveforms that use each of these indices once and only once, since there are $N!$ permutations of the N elements or, equivalently, $N!$ distinct frequency index sequences. Some of these permutations give rise to waveforms with ambiguity functions that are very different from that of the stepped frequency approximation to the linear FM chirp. For the purpose of comparison, we consider two such waveforms, the 16-chip stepped linear FM waveform, and the 16-chip Costas waveform (20). Before we do this, we introduce the notion of the *sidelobe matrix.*

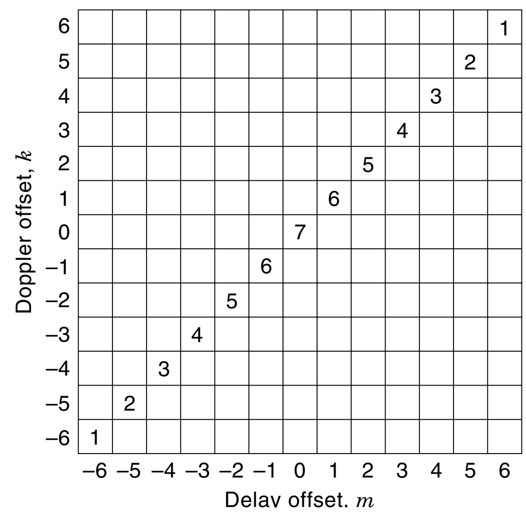

Figure 10. Ambiguity matrix of the 7-chip stepped frequency chirp having frequency index sequence (0, 1, 2, 3, 4, 5, 6).

The sidelobe matrix gives the heights of the major sidelobes of a frequency coded waveform. These can be shown to occur at locations $(\tau, \nu) = (mT, k/T)$, where m and k are integers. The sidelobe matrix is a table of the relative heights of $|\Gamma_s(mT, k/T)| = |\chi_s(mT, k/T)|$ for integer values of m and k in the range of interest. So, for example, the sidelobe matrix of a 7-chip stepped linear FM chirp having frequency index sequence (0, 1, 2, 3, 4, 5, 6) is shown in Fig. 10, whereas that for a 7-chip Costas waveform with frequency index sequence (3, 6, 0, 5, 4, 1, 2) is shown in Fig. 11. Blank entries in the sidelobe matrix correspond to zero. Clearly, there is a significant difference between the ambiguity matrices (and hence ambiguity functions) of these two frequency coded waveforms, despite the fact that they have the same duration, same number of chips, and same set of modulating frequencies. It is only the order in which the modulating frequencies are used that determines their ambiguity behavior.

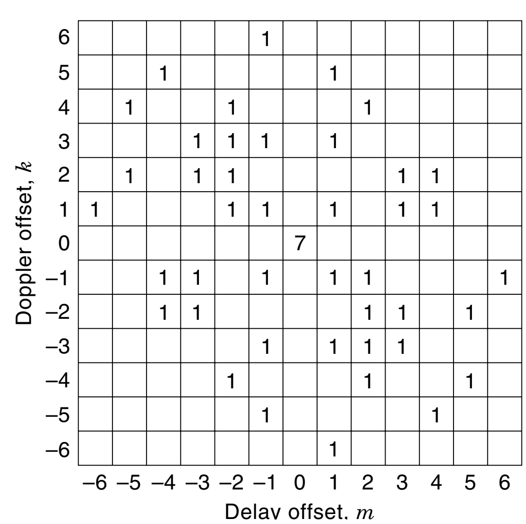

Figure 11. Ambiguity matrix of the 7-chip stepped frequency coded Costas waveform having frequency index sequence.

In looking at the ambiguity matrix of the Costas waveform in Fig. 11, it is apparent that from the point of view of both mainlobe delay-Doppler resolution and sidelobe delay-Doppler ambiguity, the Costas waveform is nearly ideal. All of the main sidelobes have a height of 1, while the mainlobe has a height of 7. In fact, by definition, an N-chip Costas waveform is a frequency coded waveform with a frequency index sequence that is a permutation of the numbers 0, 1, 2, . . ., $N - 1$ such that the mainlobe entry of the ambiguity matrix is N, while the maximum sidelobe entry is 1 (20). Sequences $(d_0, \ldots, d_{N-1})$ yielding Costas waveforms can be found for arbitrary N by exhaustive search; however, this becomes a computationally intense task, because the number of N-chip Costas sequences grows much more slowly in N, than $N!$, the number of N-chip frequency coded waveforms. For large N, this approach becomes impractical. More efficient techniques for constructing Costas waveforms are discussed in Refs. 21 and 22. One very efficient technique for constructing Costas waveforms of length $N = p - 1$, where p is a prime number, is the *Welch algorithm,* which involves a simple iteration having computational complexity proportional to N.

Phase Coded Waveforms. Consider an N-chip phase coded waveform with the rectangular $p_T(t)$ [here we assume $d_0 = \cdots = d_{N-1} = 0$ in Eq. (9)]:

$$s(t) = \sum_{n=0}^{N-1} p_T(t - nT)\exp\{j\phi_n\} \tag{12}$$

The sequence of phases $(\phi_0, \ldots, \phi_{N-1})$ specifies the phase angle to be applied to each of the N chips making up the waveform $s(t)$.

These waveforms are very similar to the types of waveforms used in direct-sequence spread-spectrum communications and hence are often referred to as *direct-sequence waveforms.* Most often, the set of phases considered is a finite set, such as $\{0, \pi\}$, $\{0, \pi/2, \pi, 3\pi/2\}$, or more generally $\{0, \pi/L, 2\pi/L, \ldots, (L - 1)\pi/L\}$, where the phases ϕ_n take on values from these sets, often repeating values unlike the frequency coded waveforms we considered in the last section.

One family of phase coded waveforms that have been applied to radar problems are the pseudonoise (PN) sequences or m-sequences commonly used in spread-spectrum communications (27–29). These waveforms take on values of either $+1$ or -1 on each chip, and hence the phases are taken from the set $\{0, \pi\}$. These waveforms are useful for generating very wide bandwidth signals by taking N large and T small. These sequences have excellent correlation properties and are easily generated using linear and nonlinear feedback shift register circuits. Their correlation properties give rise to sharp thumbtack-like responses when evaluated on the zero-Doppler ($\nu = 0$) axis. As a result, high resolution and low range ambiguity measurements can be made using these waveforms. These waveforms have the appearance of wideband noise when observed with a spectral analyzer and hence are hard to detect without detailed knowledge of the phase sequence $(\phi_0, \phi_1, \phi_2, \ldots, \phi_{N-1})$ and have thus been used for *low probability of intercept* (LPI) "quiet radar" systems, where it is not desired to give away the fact that the radar is in operation. It is rumored that the US B-2 Stealth bomber employs a high-resolution radar system using PN sequences of this kind (30).

There are many specialized families of phase coded waveforms, most of which have the property that they have excellent delay (range) resolution and ambiguity properties along the $\nu = 0$ axis. Many of these waveforms also have fairly good ambiguity and resolution properties off the zero-Doppler axis as well. Examples of these waveforms include those generated by Barker codes, Frank codes, and Gold Codes (see Ref. 27 for details on these and other related families of waveforms).

One final family of phase codes worth mentioning are the *complementary codes* originally introduced by Marcel Golay (31) for use in optical spectroscopy, but later adapted to radar measurement problems as well. Complementary codes are actually families of phase coded codewords. Golay originally introduced complementary codes having two codewords of equal length, with each chip taking on a value of either $+1$ or -1. The two codewords had the property that their delay sidelobes along the zero-Doppler axis exactly negatives each other, while their main lobes are identical. As a result, if there is no Doppler offset and two measurements of the same target scenario can be made independently, the properly delayed matched filter outputs can be added, and the result is a response in which the delay sidelobes are completely canceled. This results in excellent ambiguity function sidelobe cancellation along the zero-Doppler axis (32). Golay's basic idea has been extended to nonbinary waveforms, complementary waveform sets with more than two waveforms, and nonzero-Doppler offsets (18,19,26).

CURRENT AND FUTURE DIRECTIONS

While the classical theory of radar and sonar signals is in many ways mature, there are a number of interesting efforts to extend the theory and practice of radar and sonar signal design. We briefly outline a few of these.

One area that has received significant attention is the design of sets of multiple radar waveforms for use together. The simplest examples of these waveform sets are Golay's complementary sequence waveforms (31), which we have already considered, as well as their extensions (18,19,26), which we discussed in the last section. The basic idea is to make complementary diverse measurements that allow for extraction of greater information about the target environment than can be obtained with a single waveform. Another reason for designing sets of waveforms for use together is for use in multistatic radar and sonar systems, where there may be several transmitters and receivers in different locations. By allowing each receiver to listen to the returns from all transmitters, it is possible to extract much more information about the environment than is possible with a single—or even multiple—monostatic systems. For these systems to be feasible, it is important that the waveforms in the set have low cross-correlation, as well as envelope and spectral characteristics that allow for efficient amplification and transmission in real systems. In Refs. 33 and 34, designs for a family of waveforms of this type for sonar applications are considered. Another novel approach to multiple waveform imaging is Bernfeld's chirp-Doppler radar (35,36), which uses a mathematical analogy between measurement using a chirp and transmission tomography to obtain "projections" of a delay-Doppler scattering profile. These projections are then used to form a reconstruction of the delay-Doppler profile using the inverse Radon transform techniques typically employed in projection tomography.

When making measurements using sets of waveforms, the question of which waveforms from the set to transmit and in what order they should be transmitted naturally arises. This gives rise to the notion of adaptive waveform radar (37). In Ref. 38, the problem of designing and adaptively selecting waveforms for transmission to effect target recognition is considered. The approach used selects waveforms from a fixed set (designed for a particular ensemble of targets to be classified) in such a way that the Kullback–Leibler information measure is maximized by each selection.

The idea of designing radar waveforms matched to specific target tasks has also been considered. In Ref. 39, the problems of wideband radar waveform design for detection and information extraction for targets with resonant scattering are considered. It is noted that waveforms for target detection versus information extraction have very different characteristics. It is shown that waveforms for target detection should have as much energy as possible in the target's largest scattering modes, under the energy and time–bandwidth constraints imposed on the system, while waveforms for information extraction (e.g., target recognition) should have their energy distributed among the target's scattering modes in such a way that the information about the target is maximized.

BIBLIOGRAPHY

1. T. P. Gill, *The Doppler Effect,* New York: Academic Press, 1965.
2. P. M. Woodward, *Probability and Information Theory, with Applications to Radar,* London: Pergamon, 1953.
3. J. W. Goodman, *Fourier Optics,* New York: McGraw-Hill, 1968.
4. L. Cohen, *Time-Frequency Analysis,* Upper Saddle River, NJ: Prentice-Hall, 1995.
5. A. W. Rihaczek, *Principles of High Resolution Radar,* New York: McGraw-Hill, 1969; Santa Monica, CA: Mark Resources, 1977.
6. N. Levanon, *Radar Principles,* New York: Wiley-Interscience, 1988.
7. C. E. Cook and M. Bernfeld, *Radar Signals,* New York: Academic Press, 1967.
8. R. E. Blahut, Theory of Remote Surveillance Algorithms, in R. E. Blahut, W. Miller, C. H. Wilcox (eds.), *Radar and Sonar,* part I, New York: Springer-Verlag, 1991.
9. C. W. Helstrom, *Elements of Signal Detection and Estimation,* Upper Saddle River, NJ: Prentice-Hall, 1995.
10. R. A. Altes, Target position estimation in radar and sonar, generalized ambiguity analysis for maximum likelihood parameter estimation, *Proc. IEEE,* **67**: 920–930, 1979.
11. L. H. Sibul and E. L. Titlebaum, Volume properties for the wideband ambiguity function, *IEEE Trans. Aerosp. Electron. Syst.,* **17**: 83–86, 1981.
12. H. Naparst, Dense target signal processing, *IEEE Trans. Inf. Theory,* **37**: 317–327, 1991.
13. L. G. Weiss, Wavelets and wideband correlation processing, *IEEE Sig. Proc. Mag.,* **11** (4): 13–32, 1994.
14. J. R. Klauder, The design of radar signals having both high range resolution and high velocity resolution, *Bell Syst. Tech. J.,* 808–819, July 1960.
15. C. H. Wilcox, *The synthesis problem for radar ambiguity functions,* MRC Tech. Summary Rep. 157, Mathematics Research Center, US Army, Univ. Wisconsin, Madison, WI, Apr. 1960.
16. S. M. Sussman, Least-squares synthesis of radar ambiguity functions, *IRE Trans. Inf. Theory,* Apr. 1962.
17. W. L. Root, Radar resolution of closly spaced targets, *IRE Trans. Mil. Electron.,* **MIL-6** (2): 197–204, 1962.
18. C. C. Tseng and C. L. Liu, Complementary sets of sequences, *IEEE Trans. Inf. Theory,* **IT-18**: 644–652, 1972.
19. R. Sivaswami, Multiphase complementary codes, *IEEE Trans. Inf. Theory,* **24**: 546–552, 1978.
20. J. P. Costas, A study of a class of detection waveforms having nearly ideal range-Doppler ambiguity properties, *Proc. IEEE,* **72**: 996–1009, 1984.
21. S. W. Golomb and H. Taylor, Constructions and properties of Costas arrays, *Proc. IEEE,* **72**: 1143–1163, 1984.
22. S. W. Golomb, Algebraic constructions for Costas arrays, *J. Combinatorial Theory Ser. A,* **37**: 13–21, 1984.
23. O. Moreno, R. A. Games, and H. Taylor, Sonar sequences from Costas arrays and the best known sonar sequences with up to 100 symbols, *IEEE Trans. Inf. Theory,* **39**: 1985–1987, 1993.
24. S. W. Golomb and O. Moreno, On Periodicity Properties of Costas Arrays and a Conjecture on Permutation Polynomials, *Proc. IEEE Int. Symp. Inf. Theory,* Trondheim, Norway, 1994, p. 361.
25. J. Minkoff, *Signals, Noise, and Active Sensors: Radar, Sonar, Laser Radar,* New York: Wiley, 1992.
26. J. C. Guey and M. R. Bell, Diversity waveform sets for delay-Doppler imaging, *IEEE Trans. Inf. Theory,* **44**: 1504–1522, 1998.
27. D. V. Sarwate and M. B. Pusley, Crosscorrelation properties of pseudorandom and related sequences, *Proc. IEEE,* **68**: 593–619, 1980.
28. S. W. Golomb, *Shift Register Sequences,* San Francisco: Holden-Day, 1967.
29. R. J. McEliece, *Finite Fields for Computer Scientists and Engineers,* Norwell, MA: Kluwer, 1987.
30. R. Vartabedian, Unmasking the Stealth Radar, *The Los Angeles Times,* Sec. D, 1–2, Sun., July 28, 1991.
31. M. J. E. Golay, Complementary series, *IRE Trans. Inf. Theory,* **6**: 400–408, 1960.
32. R. Turyn, Ambiguity functions of complementary sequences, *IEEE Trans. Inf. Theory,* **9**: 46–47, 1963.
33. G. Chandran and J. S. Jaffe, Signal set design with constrained amplitude spectrum and specified time-bandwidth product, *IEEE Trans. Commun.,* **44**: 725–732, 1996.
34. J. S. Jaffe and J. M. Richardson, Code-Division Multiple Beam Imaging, *IEEE Oceans '89, part 4: Acoustics,* Seattle: Arctic Studies, 1989, pp. 1015–1020.
35. M. Bernfeld, Chirp Doppler radar, *Proc. IEEE,* **72**: 540–541, 1984.
36. M. Bernfeld, Tomography in Radar, in F. A. Grünbaum, J. W. Helton, and P. Khargonekar (eds.), *Signal Processing, part II: Control Theory and Applications,* New York: Springer-Verlag, 1990.
37. D. T. Gjessing, *Target Adaptive Matched Illumination Radar,* London: Peregrinus, 1986.
38. S. Sowelam and A. H. Tewfik, Adaptive Waveform Selection for Target Classification, *Proc. of EUSIP-96, VIII Eur. Signal Process. Conf.,* Trieste, Italy, 1996.
39. M. R. Bell, Information theory and radar waveform design, *IEEE Trans. Inf. Theory,* **39**: 1578–1597, 1993.

MARK R. BELL
Purdue University